Study on Reliability Assessment in Structural Analysis Considering Uncertainties

Xujie Liu *

Department of Civil & Environmental Engineering, Northeastern University, Boston, MA 02115, US

* Corresponding Author Email: liu.xuji@northeastern.edu

Abstract. This paper provides a comprehensive analysis of the structural integrity of a carport in Boston, designed to withstand a variety of distributed loads and environmental conditions. The structure was constructed primarily of ASTM A36 steel with trapezoidal triangular roof trusses that were optimized for strength and load distribution. Extensive load analysis were performed for local climatic conditions, including dead, wind, snow, and seismic loads. Structural responses, including bending moments, shear, reaction, deflections, buckling, and axial forces, were scrutinized using techniques such as Methods of Joints and internal force analysis. Uncertainty analysis involves evaluating variability and reliability under different properties, plotting Probability Density Function (PDF) and Cumulative Distribution Function (CDF) using statistical models such as lognormal and Weibull distributions, complemented by Monte Carlo simulations (MCS) in MATLAB coding. The purpose of the design and analysis is to ensure stability, safety, and compliance with building codes, especially in predicting extreme weather and seismic events in structural engineering.

Keywords: Structural analysis; uncertainties; Probability Density Function; Cumulative Distribution Function; Monte Carlo simulation.

1. Introduction

The uncertainty of the behavior of A36 steel was investigated via the finite element method in combination with the Monte Carlo Simulations (MCS) techniques [1]. The MCS method is commonly used for structural analysis. In this paper, three-dimensional prototypes were developed to investigate the physical and mechanical properties of A36 steel under transverse tensile and compressive conditions. According to the theoretical expression of structural analysis, the parabolic arch structure is the most economical to carry the maximum allowable load at the top. Based on this concept, the top chord of the arch structure is designed to be curved, but it is more complicated to construct. Trapezoidal roof trusses are closest to the parabolic moment diagram and have better mechanical properties. Due to their better mechanical properties and straight upper and lower chords, they are easy to construct and therefore are widely used in large-span buildings.

With the rapid development of the states and the growth of the population, auto ownership affordability continues to improve. Considering the number of factors motioned before, including the durability and stiffness of the building materials and the situation of the local real estate, a basic structure of carport model that can accommodate up to three domestic vehicles (6 feet width) is designed for the middle class. However, simple triangular roof trusses and rectangular roof trusses have poorer mechanical properties. Triangular roof trusses are generally only suitable for small and medium-span buildings, while rectangular roof trusses are generally used as joists or under special loading conditions. Considering the mechanical properties of the structure and the simplicity of construction, circular bars are chosen as the cross-section when designing triangular roof trusses. Comparing the durability and reliability of different materials in practical applications, A36 steel was chosen to ensure the strength of the structure and prevent fatigue.

Reliability analysis methods have evolved dramatically over the last three decades and have simulated optimization of structural probabilistic model design [2]. Because of the randomness, complexity of the applied stresses, and initial faults, it is frequently not possible to quantitatively explain the reaction of a structural system. There is no closed solution to the problem, even in cases where a mathematical model is discovered to accurately anticipate the behavior of the system. One of the most useful methods for gathering the necessary data in this situation is simulation. A unique method called simulation is employed to estimate quantities that are challenging to determine through analysis [3]. The MCS approach is one of the popular and widely utilized simulation techniques for resolving challenging engineering problems [4, 5].

In essence, MCS analysis is a way to use the sample mean to estimate the overall mean. When a statistical sampling procedure previously known as statistical sampling was first implemented using digital computers, the name "MCS" was created. MCS converts bits into meaningful rational numbers in its most basic form. A more complete continuous framework enhances the potency of MCS's discrete form. By repeating a history of suitable acts, MCS enables one to develop workable solutions to complicated issues. In this more often used form, every history generates a collection of real numbers or a real number (or a floating-point number generated on a digital computer). Algebraic functions can be produced by histories in different forms. However, the result is still the sum of the test samples divided by the number of trials [6].

2. Methodology

This paper focuses on assessing the reliability of structural designs and systems, especially in the face of uncertainties such as extreme weather events, material properties and construction variability. This paper discusses various structural analysis methods, design considerations, material selection, and risk assessment techniques used to ensure the safety and stability of building structures. In addition, it provides an in-depth look at case studies, simulations, and theoretical frameworks used to enhance structural reliability and resilience in real-world applications.

2.1. Engineering Background

The building was designed to be built on a concrete pavement, and the city chosen was Boston, Massachusetts, USA. According to 780 CMR 10th edition, the MA basic building codes [7]. Since the rainy season in the Boston area, the slope of the carport roof was adjusted to above 15° for drainage effect. The dimensions of the carport are 20 feet x 30 feet x 10 feet (LWH) with five shores at each side. The height of the roof trapezoidal triangular trusses at each end is 15 inches and height of ridge beam is 65 inches. Therefore, the roof angle is 15.52°, which can be calculated using trigonometric function, and the dimension is shown in Fig. 1. ASTM A36 steel was selected as the main material for the carport structure, considering the local climate and the cost of the project in Boston. The physical properties and mechanical properties of ASTM A36 steel will be used in the following analysis.

The cross-section area of shores in the design structure is I-shaped, with the shore dimension of $t_f = t_w = 0.5$in, height of 6 inch and width of 3.0 inch. For members and bars, the shape of the cross-sectional area is always designed to be circular. Cylindrical cross-sections provide a more uniform distribution of load carrying capacity when subjected to loads, which makes the structure more stable. Cylindrical sections are simpler and more economical to manufacture than other shapes such as rectangular or I-shaped in the shore. This means that the guaranteed structure performs the same or similarly capacity and at a lower cost. The circular radius of the cross-section is chosen to be 3.5 inches because the member BE is connected to the shore and needs to carry more loads, shear force and bending moments, so the member BE having a radius of 3.5 inches and the other members and bars have a radius of 1 inch.

At the design stage, the interior of half of the structure was designed to have five trusses connected by rods at each node which is shown in Fig. 2, but later calculations of the structural deadweight revealed that this did not comply with the conditions of the building code, and therefore the hypothesis was not valid. As a result, the trusses were reduced to three, but the length of the rods connecting the trusses was increased, thereby increasing the risk of deformation, and buckling of the load-bearing beams.

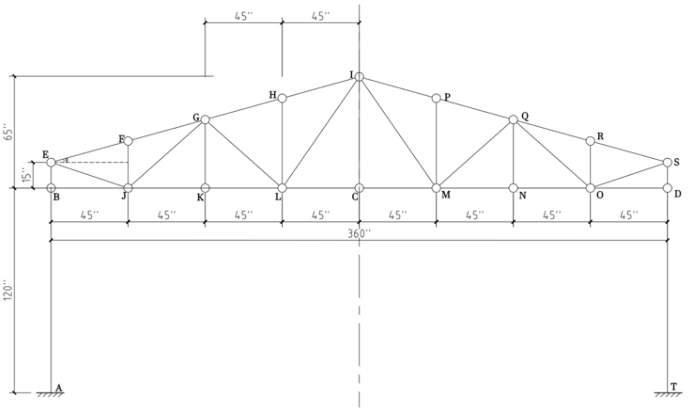

Fig. 1 Side View of Design Structure (in)

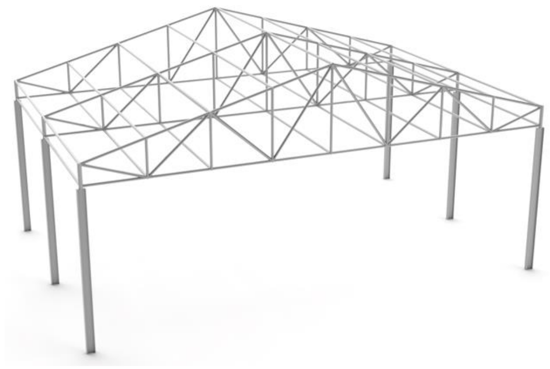

Fig. 2 3D Model of Design Structure

2.2. Structural analysis

The following eq. (1) is commonly used when calculating standard value of wind load in the main force structure,

$$\omega_k = \beta_{gz}\mu_{s1}\mu_z\omega_0 \tag{1}$$

Under the standard condition of normal atmospheric pressure 101.325kPa, temperature 15℃ and absolute dry circumstance, the unit weight of air γ = 0.012018kN/m3, and latitude 45 degrees, the gravity g at sea level is 9.81m/s2. Therefore, the basic wind pressure is 1.763kN/m2 using eq. (2), (120mph = 53.6448m/s).

$$\omega_0 = \frac{1}{2}\rho v^2 = \frac{\gamma}{2g}v^2 \tag{2}$$

The coefficient of variation of wind pressure height μ_z is first determined for a structure height of 5m (200 inches) above ground or sea level. The selected site is downtown Boston, so the ground roughness category is C, which refers to urban downtowns with dense building clusters. Therefore, the coefficient of variation of wind pressure height μ_z is 0.65. The coefficient of wind load body type is determined by the types of roofs. The type of substructure selected was a four-sided open double-pitched roof, and the roof angle so the coefficient of intermediate values go by linear interpolation in Fig. 3.

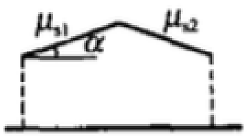

α	μ_{s1}	μ_{s2}
≤10°	−1. 3	−0. 7
30°	+1. 6	+0. 4

Fig. 3 Wind load body type and its factor

At last, the total height of the carport is round 5m, so the coefficient of gust at altitude z is not considered to calculate the standard value of wind load. This type of coefficient is assumed to be 1.0. Therefore, the standard value of wind load on the wind ward roof and the wind load on the leeward roof can be calculated. In additional, the total horizontal force induced by the longitudinal wind load on the roof is $0.05A\omega_h$ when roof angle a ≥ 30 °; $0.10A\omega_h$ when a < 30 °; where A is the horizontal projected area of the roof and ω_h is the wind pressure at height h. However, in this case, the force analysis of the structure only considers the effect of transverse loads, so the calculations are negligible for transverse effects. The wind load acts on the shores can be simply treated as the following equation based on the building code, which the design pressure is 22psf and the uniform load on each shore is 5.5plf. The wind loads applied to the support strut can be converted to point loads by applying 27.5 lbs. to points A and B respectively.

The snow load, according to the Massachusetts Building Code, the average dead load of the floor assembly shall not exceed 15 psf (720 Pa) (R301.2.2.2.1 Weight of Material), while the minimum snow load $P_f{}^1$ for flat roof is 30 psf at Boston, which can be considered as a live load. The slanted roof can be treated as flat roof as there is a snow guard. Earthquake effect causes seismic forces and base shear on the structure; the equation is used in the building code to calculate the seismic force directly on the horizontal backfill surface, the result calculated using eq. (3) is 405plf.

$$F_w = 0.100 S_s F_a \gamma_1 H^2 \tag{3}$$

Seismic shear includes both longitudinal and transverse shear because earthquake have no control over which direction it comes from. Therefore, the shear force on the carport struts due to earthquakes need to be calculated and tested in two simulations to ensure the stability and reliability of the structure. Since accurate seismic parameters and seismic coefficients could not be derived in the absence of fieldwork and simulation data, seismic load was assumed to be applied horizontally towards point B, which is 2025 pounds. Similarly, the base shear due to seismic load were assumed to be applied horizontally towards point A with same value.

2.3. Uncertainties

Furthermore, considering the uncertainties analysis. The bearing capacity of A36 steel includes cross-sectional size and material strength. Since the design structure cannot be tested to identify the performance of the material in the lab with an experiment, it is assumed that the material and section of the A36 steel specimen in the carport are accurate, and the physical and mechanical properties are used for further calculation. This assumption is necessary for the next step. On the other hand, load uncertainty is more reliable for subsequent analysis and research. In general, the common distribution models are normal distribution, lognormal distribution (LN), Weibull distribution (WBL) and gamma distribution. From the perspective of building codes, mechanical properties are usually distributed LN, and WBL is used when the data has the maximum load.

The LN depends on the mechanical properties of the material, which is the ASTM A36 Steel in this case. Since the different value of mean and standard deviation for shores and bars, there are two different values represented. The parameter μ and σ can be calculated through the following eq. (4) and (5) by the given value, the parameter of standard deviation should satisfy this range $\sigma > 0$. It should be noted that the parameters of the mean value and standard deviation are not the given values but need to be calculated by the following equations.

$$E(X) = \exp\left(\mu + \frac{1}{2}\sigma^2\right) \tag{4}$$

$$\sigma(X) = \sqrt{Var(X)} = \exp\left(\mu + \frac{1}{2}\sigma^2\right) \cdot \sqrt{exp(\sigma^2) - 1} \tag{5}$$

The equations above can be transformed into the parameters of LN as such:

$$\mu = \ln\left(\frac{E(X)}{\sqrt{1+\frac{\sigma(X)^4}{E(X)^2}}}\right), \sigma = \sqrt{\ln\left(1 + \frac{\sigma(X)^4}{E(X)^2}\right)} \tag{6}$$

Parameters are plugged into eq. (7) to calculating the Probability Density Function (PDF) $f(x)$ for the $LN(\mu, \sigma)$, which the bounds are $x > 0$.

$$f(x) = \frac{1}{\sqrt{2\pi}\sigma x} \exp\left[-\frac{(lnx-\mu)^2}{2\sigma^2}\right] \tag{7}$$

The Cumulative Distribution Function (CDF) $F(x)$ for the LN does not have a closed form solution. It can be solved by transforming into another space and using the standard normal distribution to get the results.

$$F(x) = \Phi\left(\frac{lnx-\mu}{\sigma}\right) \tag{8}$$

A WBL is always used when maximum load data is present. This is similar to use the method to do the calculation LN. The range of both parameter k and λ are greater than 0. The eqs. (9) and (10) for the expected value and standard deviation for Weibull distribution WBL (k, λ) are shown.

$$E(X) = k\Gamma\left(1 - \frac{1}{\lambda}\right) \tag{9}$$

$$\sigma(X) = \sqrt{Var(X)} = k\sqrt{\Gamma\left(1 + \frac{2}{\lambda}\right) - \Gamma^2\left(1 + \frac{1}{\lambda}\right)} \tag{10}$$

And the eq. (11) and (12) to calculate PDF and CDF of WBL using the parameters, which the bounds are $x > 0$.

$$f(x) = \frac{\lambda}{k}\left(\frac{x}{k}\right)^{\lambda-1} \cdot \exp\left[-\left(\frac{x}{k}\right)^{\lambda}\right] \tag{11}$$

$$F(x) = 1 - \exp\left[-\left(\frac{x}{k}\right)^{\lambda}\right] \tag{12}$$

2.4. Monto Carlo Simulation

MCS has been widely used to accurately estimate the reliability of engineering components and systems. However, for highly reliable systems the computational cost might be prohibitive [8]. In the simulation, it is required to use true values, which is based on the calculation and results shown in the results section. MCS uses random numbers generated by software such as MATLAB to calculate the probability of a system failure in the designed structure. Shear force V, bending moment M and axial force P are selected as comparable simulations for this scenario where LN is used for shear force and bending moment and WBL is used for axial load. The results of uncertainties including figures and tables are illustrated clearly, which is similar to the arrangement in this simulation. The LN is usually used to represent the mechanical properties of the material, while the WBL is used to represent the maximum load. The random numbers of two distribution models are generated by MATLAB software.

$$P = \frac{nf}{n} \tag{13}$$

In MATLAB MCS, the value calculated by mechanical properties is used as the maximum allowable value before system failure. And then, using the parameters calculated in the uncertainties to plug into the random function, which is shown in Table. 7. To ensure the reliability of the simulation, the total number of attempts was chosen to have 1 million samples by the function “lognrnd” and “wblrnd”, and the probability of system failure was calculated as a percentage of the total number of failures.

3. Results and Discussion

3.1. Load and Structural Analysis Results

Since this is a carport, nothing else will be placed on the roof, such as garbage or heavy objects. Therefore, the deal load of this only encompasses the structural deadweight. The total volume of the trapezial triangular truss is 31252.0 in^3. The density of ASTM A36 steel is 0.284lb/in^3. Total structural deadweight G (without shores) is 8875.6lbs. According to the Massachusetts Building Code, the average dead load of the floor assembly shall not exceed 15 psf (720 Pa) [7]. Therefore, the maximum dead load is 9000lbs, which is larger than the structural deadweight calculated. Therefore, the structural deadweight is allowed by calculation.

The results of structural analysis are shown in Table 1 for the mechanical properties of moment of inertia (MOI), section modulus W, maximum allowable bending moment M, static moment of area Q, ideal maximum allowable shear force V and maximum allowable buckling force P.

Table 1. Results of Maximum Allowable Properties

Formwork		L (in)	MOI (in^4)	W (in^3)	M (lb-in)	Q (in^3)	Ideal V (lb)	P_{cr} (k)
Shores		120.0	27.958	9.3	338295.8	5.6878	67837.4	248.6
Members	BE	15.0	117.9	33.7	228079.6	16.1	118019.2	15985.5
	IL	79.1	3.1	0.8	28510.0	0.4	9634.2	36.0
Bars		58.0	3.1	0.8	28510.0	0.4	9634.2	16.1

3.2. Maximum Bending Moment M and Shear Force V

During the structural analysis, the structure of the top of the carport can be seen as consisting of several individual beams, which is no longer treat that part as a truss. Therefore, there are bending moment M and shear force V when the beam is analyzed. Shear force exists when the internal force acts on the cross-section of the beam and the bending moment is the sum of moment caused by the resultant of the internal normal force. Calculating the bending moment carrying capacity of the shore, beams and bars based on the mechanical properties. First is to calculate the section modulus W and moment of inertia I of the steel shore and bars in the design structure. In the following eq. (14), y is the distance between the center of gravity of the section (centroid) and the force surface.

$$W = \frac{I}{y} \;\; \& \;\; M = Wf \tag{14}$$

Through the following formula, using the yield strength of A36 STEEL to calculate the bending moment, which is the maximum allowable moment of beams is 228079.6lb-in and shores is 338295.8 lb-in. The ideal maximum moment of the member EF with the maximum distributed load on the roof is 7284.5lb-in and on the shore is 61587lb-in using eq. (15). Therefore, the maximum possible moment applied to the shores and bars are allowable.

$$M_I = \frac{\omega {l_c}^2}{8} \tag{15}$$

The shear force V can be easily calculated by using the shear modulus G of A36 STEEL, which assumes the maximum elongation is 20%, the equation can be used in this scenario as the edges of the cross section are parallel to the y-axis and the shear stress is uniform across the cross section. The result is 118019.2kip. Ideal maximum shear force for member IL is 1056.1lb. Same as the value in shore, the ideal shear force is much smaller than the maximum allowable shear force of the mechanical properties.

3.3. Reaction and Deflection

The point loads and distributed loads calculated above to do the force analysis. Since points A and T are connected to the ground, the reaction force at point T is 4527.2lb, which can be calculated first if the moments at point A are assumed to sum to zero. Since the sum of the forces in the perpendicular (y) direction is 0, the reaction force at point A is 3809.5lb. Considering the distributed wind load on shore AB, using eq. (16) to calculate the maximum deflection of the strut at center, which the distributed load on shore includes wind load and seismic load. The ideal deflection on the shore is 0.1139 in.

$$\Delta_{max} = \frac{5\omega l^4}{384EI_{AB}} \tag{16}$$

The maximum deflection of A36 steel should not be exceed L/360, so the allowable deflection is 0.33in. Comparing these values, the structure remains reliable. Same method to calculate the maximum deflection of bars and beams, (ex. maximum distributed load applied on member FG), the result illustrates the same conception. Therefore, the maximum deflection of shore and bars is smaller than the allowable deflection. The structure is stable and reliability through calculation.

3.4. Method of Joints

When trying to determine, forces and states (tension and compression) or all truss members. The method of joints is appropriate. A section is cut or taken a section from the truss to solve the force and state of the determined member and use equilibrium equations. This method is used to analyze the force and states of each joint.

3.5. Internal Force Analysis

The distributed loads (including wind and seismic loads) applied to the strut can be equally divided into two equal parts at each end. The results in Table 2 show the forces and state of the members at the top for the extreme cases of the earthquake, using the method of joint as force analysis, including the date being used. Furthermore, the internal force in member DT need to be released as the structure is statically indeterminate with 1 degree of freedom.

Table 2. Force and State of each member in the truss and shores

Member	Load P (lb)	State	Virtual Load n	Length (in)	**PnL**	$\mathbf{n^2L}$
BE	3809.5	C	1.0	15.0	57142.4	15.0
EF,FG,GH,HI	2464.9	C	-1.7	46.7	-195511.5	134.7
IP,PQ,QR,RS	2464.9	C	-1.7	46.7	-195511.5	134.7
EJ,OS	2503.4	T	-1.7	47.4	-204827.4	141.1
JG,GL	618.0	T	-0.8	60.2	-30549.9	40.6
GH,HI	2464.9	C	-1.7	46.7	-195511.5	134.7
IL,IM	962.9	T	-0.7	79.1	-50499.8	34.8
MQ,QO	143.4	T	-0.8	60.2	-7087.3	40.6
SD	1894.8	C	1.0	15.0	28422.5	15.0
Sum	-	-	-	-	2668920.4	2038.3

The deformation of the truss is only an axial force, so for member DT it is assumed that there is a downward applied 1-kip force at point D in the truss. The compatibility equation is used to release the internal force between point D and shore. The determination of the axial forces for each member are shown in Table 2. Finally, the redundant force can be figured out by calculating, which the final deformation Δ is 0.

$$\delta + f \cdot X = \Delta = 0 \tag{17}$$

$$F_{DT} = X = -\frac{\delta}{f} = \frac{2668920.4}{2038.3} = 1309.4lb$$

3.6. Buckling Force

Buckling analysis is mainly used to study the stability of a structure under a specific load and determine the critical load of a structure. Linear buckling of a structure is used to obtain the potential of a structure to buckle under a special load, and the load that a structure can bear before it becomes unstable, or collapses can be estimated. Assume the structure is braced for horizontal stability. The equation of buckling force is,

$$P_{cr} = \frac{\pi^2 EI}{l^2} \tag{18}$$

The results of all members are shown in Table 2. Comparing the load number P of each member calculated individually, which is calculated by method of joints, the affordable buckling force is much larger than that in the design structure.

3.7. Mean and Standard Deviation

The mean and standard deviation of the shear force V, bending moment M and load P are listed below, using the data in Table 3. Coefficient of Variance (CoV) is the ratio between the standard deviation and the mean, which is a statistical measurement. The higher value of CoV means the greater level of dispersion around the value of mean

Table 3. Results for mean and standard deviation (V, M, P)

	Shear Force V		Bending Moment M		Axial Load P	
	Bar	Shore	Bar	Shore	Bar	Shore
Mean	675.71	731.45	6329.15	14221.41	1407.78	1566.10
S.D.	165.11	316.37	965.43	19527.38	1002.25	1170.70
CoV	0.2444	0.4325	0.1525	1.3731	0.7119	0.7475

3.8. Lognormal Distribution

The parameters of mean and standard deviation are used to calculate the PDF and CDF by eq. (7) and (8). The results of data are shown in Table 4 and the PDF and CDF diagrams are shown in Fig. 4 & 5, which the X range for the bar and shore is $0 < X \leq 10$ with a 0.01 separation. The procedure is done in MATLAB software.

Table 4. Parameters Results in LN (bar and shore)

LN (bar)				LN (shore)			
μ	3.760673642	E(X)	675.707601	μ	1.67620820	E(X)	731.448184
σ	3.15982502	σ(X)	165.111951	σ	3.13650066	σ(X)	316.368898

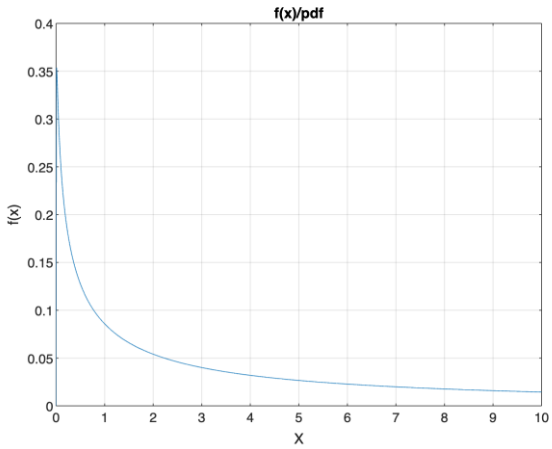

Fig. 4 PDF of LN on bar

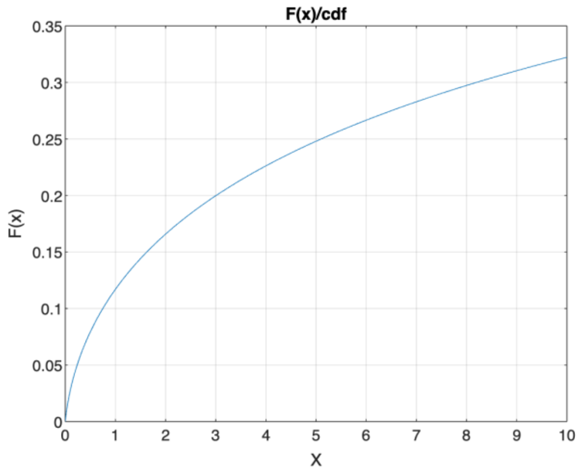

Fig. 5 CDF of LN on bar

The range used in MATLAB and analytical method are the same when using the parameters of bending moment M. Fig. 6 & 7, and Table 5 list the results.

Table 5. Parameters Results in LN (bar and shore)

LN (bar)				LN (shore)			
μ	3.7658059	$E(X)$	6329.14681	μ	-0.63413781	$E(X)$	14221.4116
σ	2.23705529	$\sigma(X)$	965.428817	σ	4.51589233	$\sigma(X)$	19527.3801

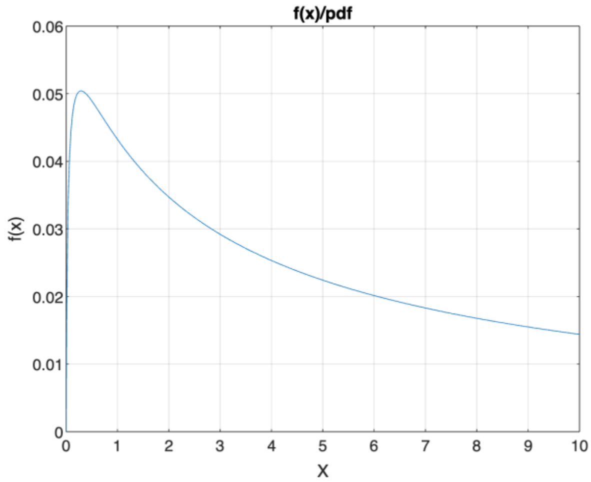

Fig. 6 PDF of LN on bar

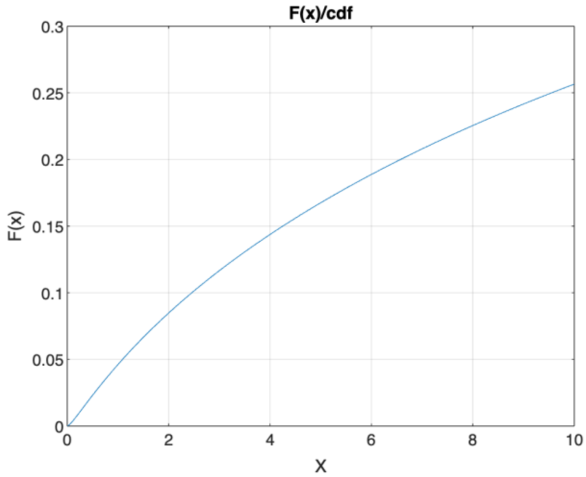

Fig. 7 CDF of LN on bar

In these figures, μ is a scaler parameter and σ is a shape parameter. Through the definition of a LN, it is a right-skewed continuous probability distribution, which means it has a long tail to the right. In these figures obtained by parameters, the shape and curve meet the basic requirements of LN. When modeling random variables that might vary by multiple orders of magnitude, the LN is frequently utilized. The LN is widely used to simulate random variables that arise from the multiplication of numerous independent variables. The following eq. (18) about error factors are a few applications that use LNs [9].

$$EF = \sqrt{\frac{95th\ percentile}{5th\ percentile}} = \frac{95th\ percentile}{50th\ percentile} = \frac{50th\ percentile}{5th\ percentile} \tag{19}$$

When using the mean and standard deviation as inputs to a LN, both input parameters must be positive, and the error factor must be greater than 1. Reliability and related fields are where survival functions are most frequently applied. The probability that the variate takes a value larger than x.

3.9. Weibull Distribution

The procedure is similar to the LN in MATLAB, wblpdf (x,k,λ) and wblcdf (x,k,λ), which the range of X and separation are the same. The results are shown in Table 6 and Fig. 8 & 9.

Table 6. Parameters Results in WBL (bar and shore)

WBL (bar)				WBL (shore)			
k	1.183779527	E(X)	1.17069398	k	1.1227014	E(X)	1.56609637
λ	1.240105442	σ(X)	1.00224721	λ	1.63370433	σ(X)	1.40777948

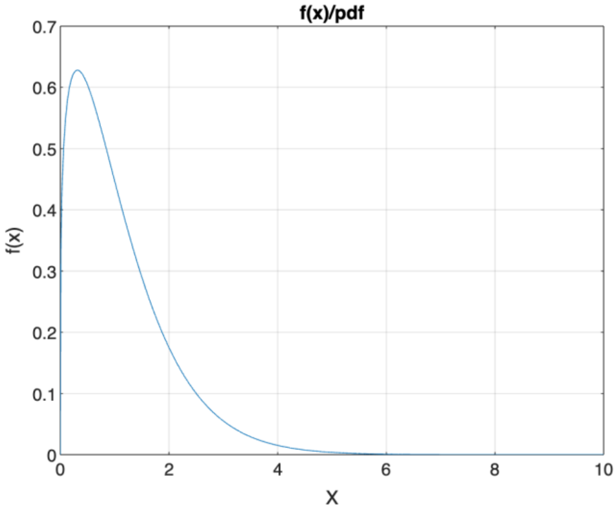

Fig. 8 PDF of WBL on bar

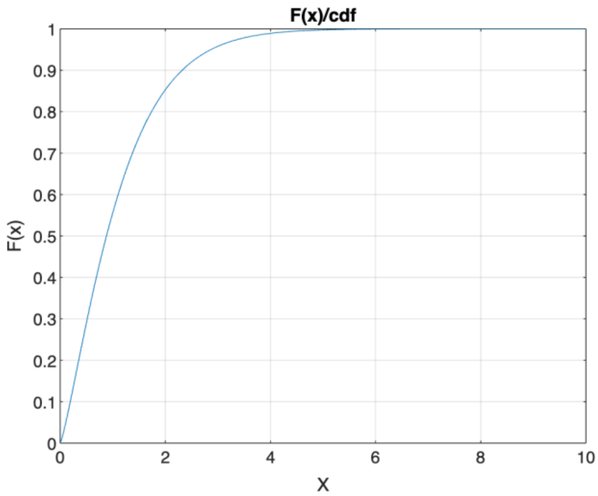

Fig. 9 CDF of WBL on bar

In WBL, the maximum load can be also treated as the value of the mode of WBL. It exists if the parameter $\lambda > 1$, otherwise no mode exists,

$$Mode = k\left(\frac{\lambda-1}{\lambda}\right)^{\frac{1}{\lambda}} \tag{20}$$

The value of parameters in Table 6 are plugged into eq. (19), then the value of mode of bar and shores are 0.315 and 0.629 respectively, which is shown obviously in Fig. 8. The PDF value of the extreme response is estimated, and the CDF figure is easily obtained by one-dimensional integration in a specific distribution range.

3.10. Monte Carlo Simulation

For the hypothesis, the shape of the cross-section area of shore of design structure is I-shaped, which means very high MOI comparing to the members and bars, even the ideal max calculated is too large than the maximum value calculated in the true scenarios. Therefore, only considering the shear force, bending moment and axial load of the members and bars. In Table 7, the ideal max is calculated by the mechanical properties, which the process is shown in the equation below.

Table 7. Parameters and Comparable Maximum Values in MCS

Uncertainties	LN				WBL	
Properties	Shear Force V		Bending Moment M		Load P	
Member	Bar	Shore	Bar	Shore	Bar	Shore
Scalar	2.818	1.676	3.766	-0.634	1.184	1.123
Shape	2.719	3.137	2.237	4.516	1.240	1.634
Ideal Max	118019.2	67837362.6	1222364.2	338295.8	16.1	248.6

Finally, the resultant diagrams of Probability of Failure versus Number of Samples by MCS are plotted by the MATLAB, as shown in the Fig.10. Through Fig. 10, after 1,000,000 trials, the probability of failure tends to be relatively uniformed, this shape naturally illustrates the phenomena in the design structure, which the probability of failure of the axial load or called buckling part is even 0. However, the results of both shear force and bending moment are overlapped in the most of times. And the resultant probability of failure is approximately 0.0005, which means on average after 2000 trials, the structure will failure, which reaches the initial thoughts that the results of MCS should be in the range of one in a thousand and one in ten thousand. Although in this case, since this is a design-structure experiment, there is no actual data or contextual support in all aspects, and the results are more inferred from assumptions and calculations. Therefore, the probability of structural failure concluded in this way is naturally theorized and idealized.

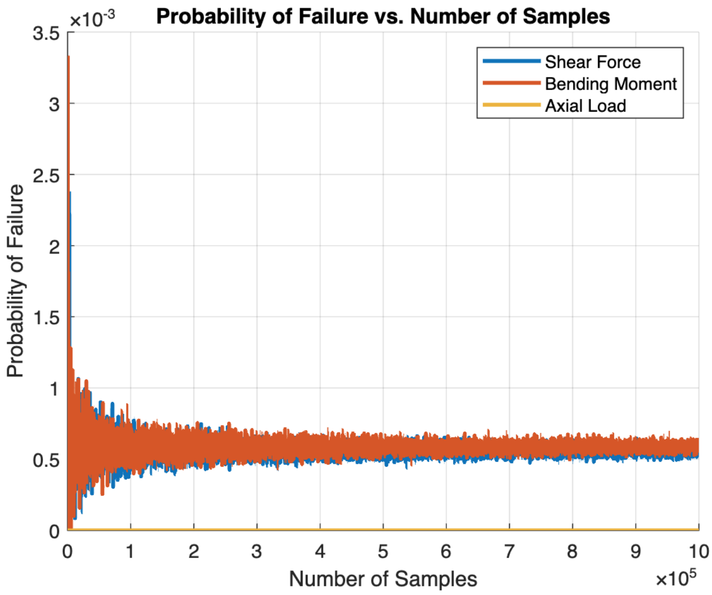

Fig. 10 MCS Results

Reinforcing bars in trusses are generally not I-beam shaped, and in actual engineering applications, I-beam shaped reinforcing bars are seldom used in steel trusses. In practical engineering applications, I-beam bars are rarely used in steel trusses. This results in the steel bars in the structure having relatively high value of MOI and small cross-sectional area, which in turn leads to a larger calculated value of the ideal maximum. Therefore, after the first calculation, the designed structure was re-designed and re-calculated by adjusting the cross-sectional shapes and sizes of the members and bars in the structure, which resulted in the present more reliable results. Meanwhile, due to the lack of experimental data support, the data calculated is not so reliable and accurate as shown in the diagram and results because of so many assumptions made in the calculations, especially the distributed live loads on the roof.

Furthermore, this is the reason why so much padding was done before, especially the uncertainty part, to present the structural forces by simplifying the model and the distribution of uncertainties. Simpler material models are used to approximate complex material behavior. For example, use linear elastic material properties for materials that exhibit nonlinear behavior over the expected load range. Validate simplified models against experimental or benchmark data to ensure that they provide results within acceptable error limits is another reliable method.

As a result, probability space's coarse and fine division is enhanced. Only a limited number of candidate samples must be analyzed throughout the adaptive sampling process, which can greatly increase training efficiency and prevent the issue of inadequate computer memory [10].

4. Conclusion

This lengthy study demonstrates a commitment to ensuring stability, safety, and compliance with building regulations. The airport was specifically designed to meet Boston's harsh climatic conditions, and it embodies the rigor of structural engineering analysis. Given the lessons of previous catastrophic roof collapses, the study encourages the use of ASTM A36 steel, which is known for its excellent strength and durability and can handle a variety of stressors, including wind, snow, and seismic loads. Based on the analysis of the collapsed garage, the A36 steel truss structure was constructed and installed.

The calculation and analysis process of structural uncertainty are fully explained through a series of steps like internal force analysis, material selection, probability distribution model using different types of load uncertainty, and sampling simulation risk analysis. This gives a certain reference for the risk analysis of truss structures. It also exemplifies all of the benefits that A36 steel has to offer. The study material in this work offers a certain reference for structural design and risk assessment in the event of extremely severe weather, based on fundamental safety standards and conditional assumptions.

When integrated with traditional structural analysis techniques like internal force analysis and the node method, the design's uncertainty is thoroughly investigated in an effort to achieve accuracy. Because lognormal and WBLs offer valuable insights into the strength and carrying capacity of materials, they must be used to simulate different types of uncertainty. The Massachusetts Building Code's safety tolerances for various loads are satisfactorily met by the proposed building. Two probability distribution models, the WBL, and the LN, are used to assess the design structure's stability under extreme weather scenarios. MCS method is used to predict an appropriate failure probability, boosting trust in the design's dependability and offering more proof of the structure's sturdiness.

In general, this paper recommends testing and monitoring after build to ensure that theoretical predictions are consistent with actual performance and emphasizes the need for caution. In addition to validating the model's predictions, these measures will ensure the long-term safety and functionality of the structure. This study is based on a deep understanding of structural design and analysis combined with a skilled handling of uncertainties that arise during the design process. By applying sophisticated statistical models and probabilistic analysis to assess the resilience of structures to harsh environments, it supports the notion that good engineering should go beyond mere compliance with regulations to anticipate future problems.

References

[1] Wu G, Shen Y, Fu F, Guo J, & Ren H. Study of the Mechanical Properties of Wood under Transverse Compression Using Monto Carlo Simulation-Based Stochastic FE Analysis. Forests, 2022.

[2] Morris B. The components of the Wired Spanning Forest are recurrent. Probab Theory Relat Fields 125, 259–265, 2003.

[3] Gordini M, Habibi M R, Tavana M H, TahamouliRoudsari M, & Amiri M. Reliability Analysis of Space Structures Using Monte-Carlo Simulation Method. Structures (Oxford), 14, 209–219, 2018.

[4] Melchers R E, Beck AT. Structural Reliability Analysis and Prediction John Wiley & Sons, 2017.

[5] Kamyab M R & Fadaee M J. Reliability assessment of structures by Monte Carlo Simulation and Neural Networks, 2012.

[6] Dunn W L William L & Shultis J. Kenneth. Exploring Monte Carlo methods. Elsevier, 2012.

[7] Mass.gov, 780 CMR TENTH EDITION MASSACHUSETTS AMENDMENTS, Chapter 16: Structural Design. Page 167, 2021.

[8] Der Kiureghian, A. Risk and reliability analysis: theory and applications : in honor of Prof. Armen Der Kiureghian (P. Gardoni, Ed.). 2017.

[9] Modarres, M. (Mohammad), & Groth, K. Reliability and risk analysis (Second edition.). CRC Press. 2023.

[10] Jin Zhou, Jie Li. An enhanced method for improving the accuracy of small failure probability of structures, Reliability Engineering & System Safety,Volume 228, 2022, 108784, ISSN 0951-8320, 2022.